Future Technology
Open Access Journal
ISSN 2832-0379

August 2025| Volume 04 | Issue 03 | Pages 216-226

Journal homepage: https://fupubco.com/futech

https://doi.org/10.55670/fpll.futech.4.3.20

Future Publishing LLC

Article

Optimization of small submersible pressure hull based on MOGA

Xiaoyu Liu[1,2], *Aldrin D Calderon[1,2] Xiangyao Wu[3]

[1]School of Mechanical, Manufacturing, and Energy Engineering, Mapua University, Manila, Philippines
[2]School of Graduate Studies, Mapua University, Manila, Philippines
[3]Equipment Management Department, DongFang International Container (Qingdao) Co., Ltd. Qingdao, China

ARTICLE INFO

Article history:
Received 25 April 2025
Received in revised form
08 June 2025
Accepted 17 June 2025

Keywords:
Finite element analysis, Optimization, Moga algorithms

*Corresponding author
Email address:
yanqi1015@126.com

DOI: 10.55670/fpll.futech.4.3.20

ABSTRACT

This study presents the structural optimization of a small-scale Autonomous Underwater Vehicle (AUV) designed for shallow-water marine aquaculture applications, such as monitoring water quality and the living conditions of farmed species. A cylindrical pressure hull model was developed using ANSYS Workbench and analyzed under a constant pressure of 0.5 MPa. Latin Hypercube Sampling (LHS) and Multi-Objective Genetic Algorithm (MOGA) were employed to optimize three key design variables: shell thickness, inner radius, and length. The final optimized design resulted in a 54.78% reduction in hull mass, a 25.25% decrease in maximum deformation, and maintained stress levels well below the allowable limit of 328 MPa. The optimization process significantly enhanced the AUV's structural efficiency, safety, and agility, offering valuable insights for the design of lightweight submersible structures in practical environments.

1. Introduction

Utilization in international public sea areas. Structural optimization plays a crucial role in improving their performance, reducing manufacturing costs, and enhancing adaptability in complex marine environments. With the advancement of computational methods, Finite Element Analysis (FEA) and optimization algorithms have become standard tools in structural design. Numerical approaches based on FEA facilitate efficient simulation and structural evaluation, while modern optimization algorithms like the Multi-Objective Genetic Algorithm (MOGA) support performance trade-off analysis.

1.1 Literature review with problem statement

Recent research has laid a solid ground for the structural optimization of submersible pressure hulls, especially with regard to simulation, lightweighting, and advanced manufacturing. Corpuz et al. [1] utilized CFD modeling to enhance industrial filtration systems, demonstrating the promise of simulation-based optimization. Li and Calderon [2] analyzed trends in precision cutting, providing insights into sophisticated fabrication processes that can be applied to submersible parts. Liu and Calderon [3] carried out CFD-based optimization of filter housings, providing methodologies applicable to shell airflow and pressure properties. Liu et al. [4] computed pre-stressed modal characteristics of ship anchor components, showing how modal analysis underload can improve structural reliability. Macreadie et al. [5] highlighted the use of ROVs in deep-sea exploration, which indirectly provides design specifications for rugged submersible hulls. Prabhakar and Buckham [6] derived a dynamic ROV tether model, applicable to the integration of structural and control aspects. Robles et al. [7] introduced a bio-inspired aerodynamic structure based on CFD, providing techniques for environmental adaptability in underwater engineering. Wei et al. [8] introduced testing algorithms, which are critical in guaranteeing the integrity of pressure hulls manufactured. Zhang and Calderon [9] addressed the evolution of CNC lathes and their relevance to the precision manufacturing of submersible components. He et al. [10] treated the use of lightweight pressure shell design by means of Kriging modeling and multi-objective optimization, with resultant strength increases and weight savings. Chen et al. [11] combined CFD simulation and genetic algorithms to minimize AUV shapes, making use of Latin Hypercube Sampling (LHS) for efficient design. Imran et al. [12] conducted nonlinear buckling analysis of composite spherical pressure hulls, confirming their structural strength through finite element analysis.

Xu et al. [13] simulated deep-sea pressure-resistant cabins using FEA, offering methods transferable to electronic module protection. Dama et al. [14] discussed lightweight body-in-white design for automotive bodies, tracking the objectives of marine lightweighting. He et al. [15] also applied Kriging-based optimization to underwater pressure hulls, providing conference-level experimental evidence of a 5.9% mass reduction and a 22.97% strength increase. Wang et al. [16] conducted a strength analysis of vehicle frames, providing a baseline for research on stress distribution and load path optimization. However, previous studies have primarily focused on single-objective optimization or lacked the integration of Latin Hypercube Sampling with finite element modeling and MOGA. Moreover, few works have addressed small-sized pressure hulls operating in shallow waters. This study fills that gap by proposing a unified framework that combines LHS, FEA, and MOGA for designing lightweight and robust hulls.

1.2 Research objectives

The primary objective of this research is to optimize the structural design of a small submersible pressure hull used in shallow-water Autonomous Underwater Vehicles (AUVs), with the goal of achieving lightweight construction without compromising structural integrity and operational safety. Design and simulation of the pressure hull using Finite Element Analysis (FEA) to evaluate deformation and stress under 0.5 MPa pressure. Application of Latin Hypercube Sampling (LHS) to generate diverse sample points for varying design parameters. Use of Multi-Objective Genetic Algorithm (MOGA) to simultaneously minimize mass, deformation, and equivalent stress. Validation of the optimized design through structural safety analysis and resonance frequency checks. Quantitative evaluation of optimization outcomes, including percent reduction in mass and deformation. This integrated optimization approach provides a robust methodology for improving the endurance and operational efficiency of small-scale AUVs used in marine environments.

2. Design of parameter variables for pressure hulls

2.1 Structural and dimensions of AUV

Based on these considerations, a streamlined body structure AUV is selected, as shown in Figure1. The design requirements for the small AUV in this study are as follows: Navigation Speed: The AUV operating in shallow waters does not require a high navigation speed; it only needs to be able to detect marine fish and water quality conditions. Therefore, the horizontal speed should reach 2 m/s, and the vertical speed should reach 0.5 m/s.

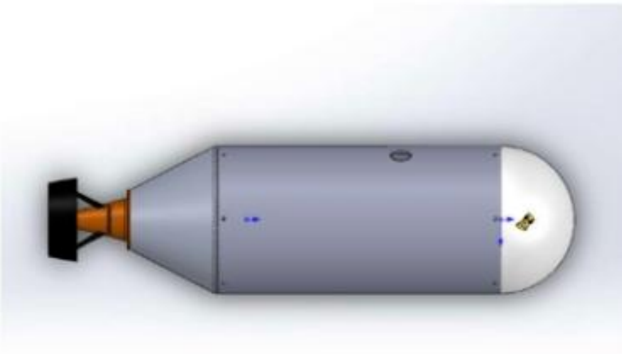

Figure 1. Streamlined body structure AUV

Size and Weight: Given that the primary purpose of this type of small AUV is ease of deployment and portability, its size and weight should not be excessive. The dimensions are set at a length of 900 mm, a diameter of 250 mm, and a weight not exceeding 50 kg. Endurance Time: To ensure effective monitoring of fish populations and water quality, the battery life should be maintained at over 2 hours. Working Depth: The typical working depth in shallow waters is around 50 meters, allowing for maximum coverage of fish activity depths. The above parameters are summarized in Table 1 as follows:

Table 1. Parameter specifications

Parameter Name	Value
Navigation Speed (Horizontal)	2m/s
Navigation Speed (Vertical)	0.5m/s
Dimensions	R=250mm,L=900mm
Weight	50kgf
Endurance Time	2h
Working Depth	50m

The density of seawater will also affect the AUV. According to the planned horizontal speed of 2m/s and the calculated propeller power, a propeller with a larger functional power should be selected, such as a propeller with an average power of 150 W. The T200Blue underwater robot propeller meets the standard. The design of the battery compartment needs to be based on the size of the battery. Selecting the right battery can improve the endurance of the submersible and enable the submersible to operate normally within the expected time. Therefore, it is more efficient to select a battery with high density, small volume, small mass, and large capacity. After comparison, lithium battery packs are more suitable as the power supply for AUVs. According to the selected thruster voltage of 12V and the required endurance of two hours, 18650-model ternary lithium batteries can be combined into a battery pack. The shape of the battery compartment is designed according to the battery size. The length of the battery compartment is 350 mm, the inner diameter is 190 mm, the base diameter is 206 mm, and the length, width, and height of the battery slot are 350 mm, 130 mm, and 100 mm, respectively. To protect the battery and reduce the heat generated during battery operation, the battery compartment can be set to a hollow shape to facilitate heat dissipation. The battery compartment and ribs are both made of SBM-045 material, which is a lightweight, easy-to-process solid composite material with low density and high compressive strength. After the battery is installed, the battery compartment can be inserted into the pressure-resistant compartment to ensure that the battery is installed without misalignment. When the battery is working normally, the hollow part of the battery compartment can dissipate heat, ensuring battery safety and extending battery life.

2.2 Assumptions and limitations

The primary materials used in the pressure-resistant hull include aluminum alloy, acrylic, and fiberglass. Due to variations in structure and material, each has different requirements for the marine environment. In the dynamic underwater environment, the AUV not only endures pressure from fluid forces but also experiences fatigue loads caused by random wave actions. Thus, materials with high strength, high fatigue limits, and low density are essential. To ensure the feasibility of optimization and simulation

within an engineering context, several assumptions were made:
Loading conditions: A constant external pressure of 0.5 MPa was applied to represent the hydrostatic pressure at a working depth of approximately 50 meters, which is typical for shallow-water AUV operations in marine aquaculture.
Material Selection: The pressure hull was designed using 7075-T6 aluminum alloy, selected for its high strength-to-weight ratio, corrosion resistance, and proven reliability in marine and aerospace applications. Mechanical properties were based on standard material data, including:
Yield strength: 505 MPa
Elastic modulus: 70 GPa
Poisson's ratio: 0.3
Allowable design stress: 328 MPa
Structural Idealization: The model assumes ideal cylindrical symmetry, uniform wall thickness, and perfect bonding of components. Effects such as manufacturing tolerances, residual stresses, and weld imperfections are not included.
Environmental effects: The simulation does not consider factors such as seawater corrosion, dynamic wave loads, or thermal gradients. These may affect long-term structural integrity and are suggested for future investigation.
Safety factor application: A conservative safety factor of S = 2.5 was adopted based on classification society recommendations (e.g., German Lloyd's rules), ensuring a sufficient margin under the design pressure (Table 2).
Following in-depth research, 7075-T6 aluminum alloy was selected as the primary material for the pressure-resistant hull. This alloy has excellent mechanical properties and chemical stability, making it suitable for hull construction. Cold-worked and high-strength forged 7075 aluminum alloy performs significantly better than low-carbon steel. It has superior stress-relaxation resistance, good plasticity, and weldability. The cylindrical pressure hull is classified into two types: long cylinders and short cylinders. The distinguishing formula for long and short cylinders in Eq:

$$L > 4.0D\sqrt{\frac{D}{2T}} \tag{1}$$

It is classified as a long cylinder; otherwise, it is classified as a short cylinder. The outer diameter range is (190 mm - 210 mm).

$$4.0D\sqrt{\frac{D}{2T}} \in (14932mm - 3666mm) \tag{2}$$

Given that 14932 mm is significantly longer than the pressure hull length L = 400 mm, it can be determined that this pressure hull belongs to the category of short cylinders. The simplified derivation of the von Mises formula yields:

$$P_{cr} = \frac{2.59ET^2}{LD\sqrt{\frac{D}{T}}} \tag{3}$$

The formula for calculating the safety factor S is:

$$S = \frac{P_{cr}}{P} \tag{4}$$

Set the sixth-order natural frequency, as shown in Figures 3-8. According to the German Lloyd's rules, the safety factor S decreases as the AUV's working depth increases. At the maximum working depth of 50 m, the safety factor S = 2.5 as shown in Table 3 (Prabhakar & Buckham, 2005).

Table 2. Safety factor and working depth

Safety Factor	2.5	2.4	2.2	2.0	1.9	1.5
Working Depth	50	100	200	300	400	1000

The safety factor in different operating water shows in Table 2 by using the Lamé equations, suitable wall thicknesses are calculated within the range of outer diameters as follows: When D=195mm and T=3mm, substituting into equation (3) yields a maximum allowable pressure of 2.581 MPa for the hull. Substituting this value into (4), the safety factor S is calculated to be 5.1>2.4. Here, the value of P is known from the previous text to be 0.5 MPa. When D=192mm and T=0.5mm, substituting into the formula gives a maximum pressure that the pressure hull can withstand of approximately 0.003 MPa, resulting in a safety factor of 0.006<2.5, which does not meet the requirements. When D=198 mm and T=4 mm, substituting into the formula yields a critical pressure of 2.928 MPa, with a safety factor of S=5.8>2.5, which meets the requirements. Therefore, this set of data is selected as the modeling data for the pressure hull.

2.3 Model and modal of FEA

Create a three-dimensional model of a cylindrical pressure hull with an inner diameter of 190 mm, a length of 400 mm, and an outer diameter of 198 mm in Workbench software. Conduct a static simulation analysis in the Model option. Select the Aluminum alloy 7075-T6 material from the material library and assign it to the model. Then, generate the mesh, fix both ends of the pressure hull, and apply a load pressure of 0.5 MPa to the hull. Once the setup is complete, perform the static analysis to obtain the total deformation plot and equivalent stress plot of the pressure hull. Finally, it was determined that, while meeting the strength requirements, the shell thickness was reduced as part of the design optimization to minimize overall structural weight without compromising strength, with a thickness of 4 mm satisfying the safety factor requirements as shown in Figure 2. The modal simulation analysis of the modal module of the pressure chamber shell in the workbench software is carried out to check whether the structural strength of the model is reasonable and avoids the resonance reaction. First, the pressure chamber shell is meshed, and the two ends are supported by adding supports, and then the model is solved to set the sixth-order natural frequency, as shown in Figures 2-Figure8.

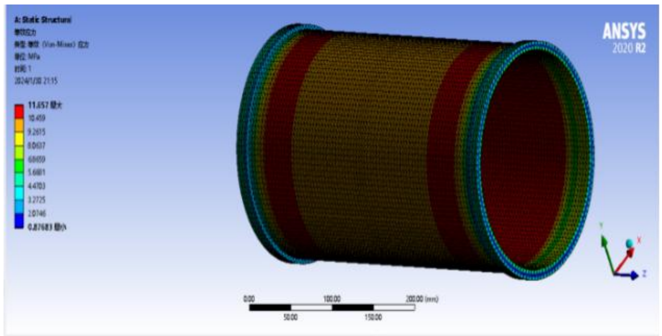

Figure 2. Total deformation and Equivalent stress of the cabin

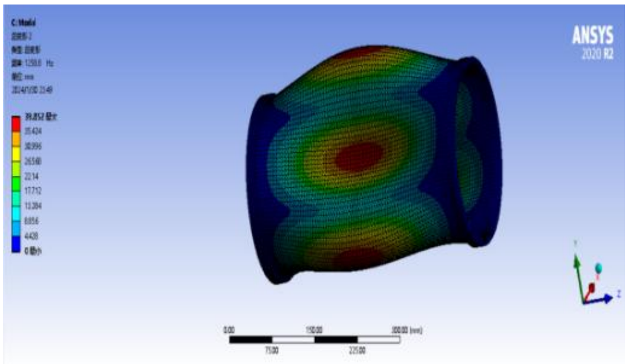

Figure 3. First-order mode shape of the cabin

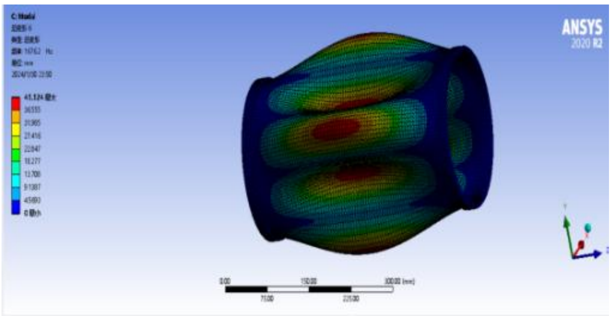

Figure 4. Second-order mode shape of the cabin

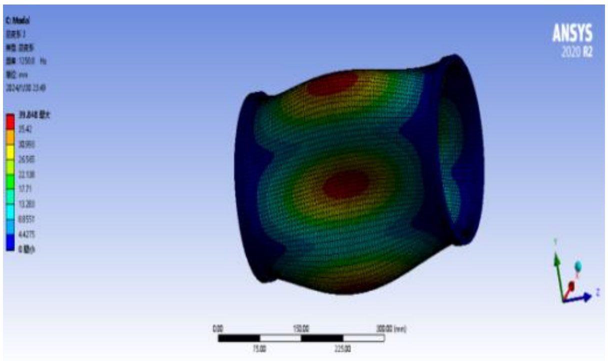

Figure 5. Third-order mode shape of the cabin

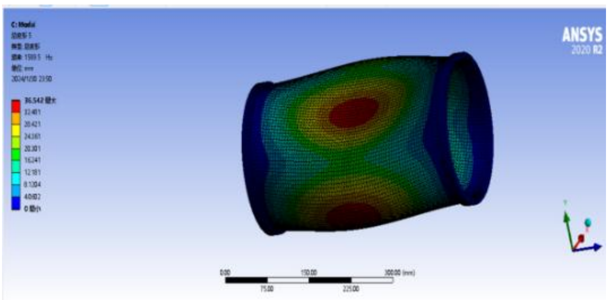

Figure 6. Fourth-order mode shape of the cabin

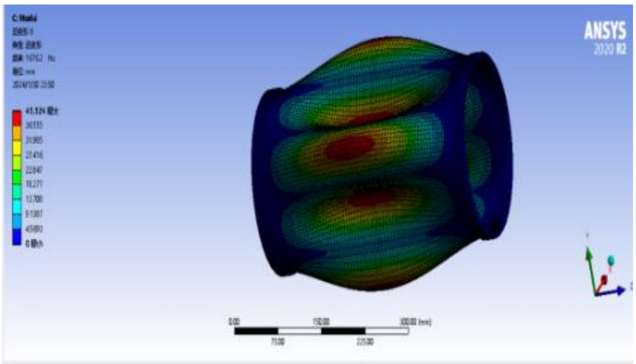

Figure 7. Fifth-order mode shape of the cabin

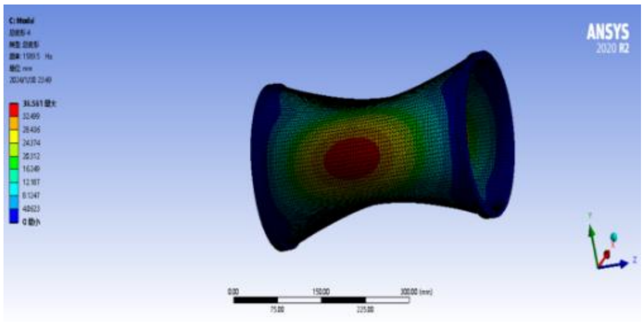

Figure 8. Sixth-order mode shape of the cabin

Table 3. Natural frequencies of each mode

Mode (Order)	First	Second	Third	Fourth	Fifth	Sixth
Frequency (Hz)	1258.8	1258.8	1589.5	1589.5	1676.2	1676.3

Table 3 shows the results from Natural Frequencies of each mode, based on the results obtained from the modal simulation of the hull, it can be observed that the first six natural frequencies of the pressure hull fall within the range of 1250-1700 Hz. Using the structural resonance frequency formula, we can calculate:

$$f = \sqrt{\frac{k}{m}} \tag{5}$$

where k is the stiffness coefficient and mm.
From Figure 9, the deformation amount can be observed. We can then use the stiffness coefficient calculation formula:

$$k = \frac{P}{\delta} \tag{6}$$

where P is the constant force causing the deformation, indicating the deformation amount. By substituting the values into the formula, we can calculate the stiffness coefficient k and then substitute it into the resonance frequency formula to find that the resonance frequency is 1823 Hz. Since the first six frequencies obtained from the simulation are all less than the resonance frequency, the designed pressure hull structure can avoid resonance response, confirming that the structure is reasonable.

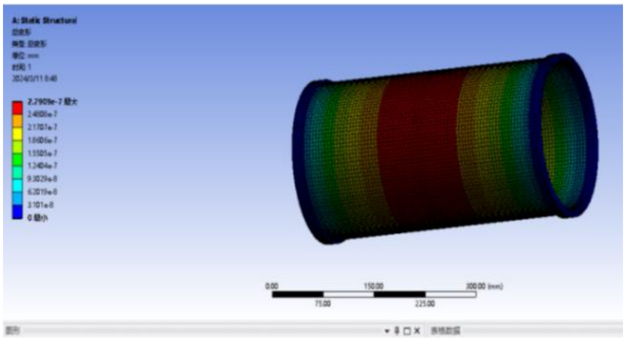

Figure 9. Deformation of the pressure hull

2.4 End cap model and pressure analysis

The calculation formula for the thickness t of the flat end cap is as follows:

$$t = \sqrt{\frac{D \cdot P}{2 \cdot y \cdot \sigma_{\text{allowable}}}} \tag{7}$$

where:

D is the outer diameter of the end cap

y is the shape factor of the end cap

σ is the allowable stress of the material.

Assuming the shape factor y = 1, the calculated thickness is t = 6.78 mm. Considering the effects of assembly and processing conditions, the thickness is taken to be approximately t = 10 mm. To ensure the stability of the end cap, a strength check and static analysis can be performed. In the ANSYS Workbench software platform, the following steps can be followed:

- Apply boundary conditions: Apply a pressure load of 0.5 MPa.
- View results after solving, review the equivalent stress contour plot, total deformation plot, and equivalent elastic strain.

It is important to note that this is just a basic overview of the process; specific situations may require further elaboration based on the actual problem. Additionally, when conducting static analysis, factors such as the mechanical properties of the materials and the geometric shape of the structure must be considered to ensure the accuracy of the analysis results, as shown in Figures 10 and Figure 11.

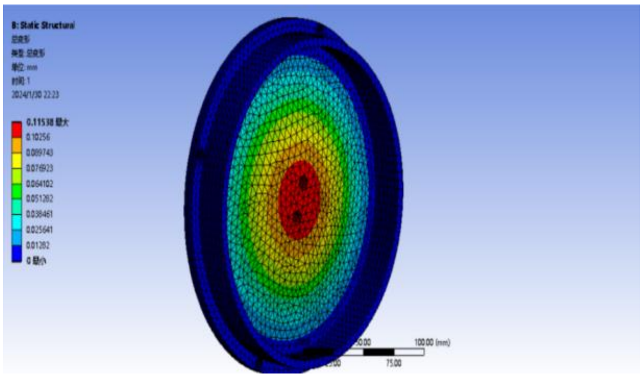

Figure 10. Total deformation cloud diagram

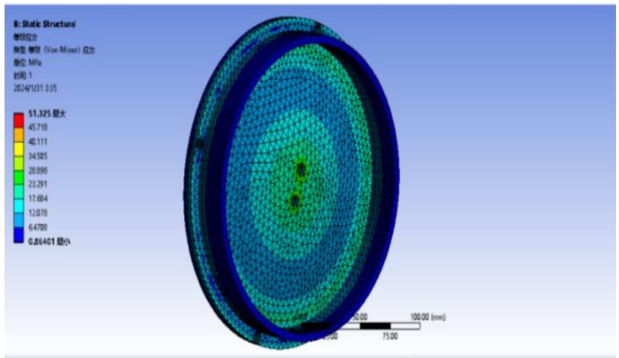

Figure 11. Equivalent stress diagram

Through the static displacement response diagram of the pressure cabin end cover, we can observe that after applying an external load pressure of 0.5MPa, the middle part of the end cover shifted by 0.115238mm, and this thickness is only 10mm, so its displacement amplitude is much smaller than the actual thickness of the pressure cabin end cover. From the equivalent stress diagram, the maximum equivalent stress borne by the pressure cabin end cover reaches 51.325MPa, while the allowable stress value of the pressure cabin material is 328MPa. In comparison, the maximum equivalent stress in the diagram is significantly lower than the allowable stress. Therefore, under the analysis of comprehensive calculation and strength test, it is determined that the 10mm thickness of the pressure cabin end cover can meet the safety factor standard, and thus, the parameter configuration is considered appropriate.

3. Optimization of AUV pressure cabin parameters

3.1 Experimental design method

With the development and refinement of computer technology and finite element theory, structural optimization design has become a highly mature research field with an increasingly broad range of applications. Currently, structural optimization design typically constructs finite element models using numerical methods, computes the results of structural optimization on computers, and proposes specific design solutions based on these results. This approach not only significantly improves engineering efficiency but also saves substantial costs. As computer technology continues to advance and computational mechanics theory evolves, structural optimization algorithms have gradually transitioned from traditional finite element methods to modern genetic algorithms, leading to wider applications in optimization design. Typically, structural optimization involves three core components: design variables, objective functions, and constraints. The objective functions mainly include performance indicators such as minimizing mass or maximizing displacement. These indicators impose mutual constraints and influence each other, making the optimization problem more complex. Design variables refer to the parameter variables that need to be adjusted and optimized during the design process, such as the geometric and physical parameters of the structure. Based on the number of objective functions, optimization problems can be classified into single-objective optimization and multi-objective optimization. Constraints are the various conditions that the optimization variables must adhere to, typically presented in the form of equations and inequalities [11]. Latin Hypercube Sampling (LHS), first proposed by McKay et al. in 1979, is mainly used in fields such as computer experiments or Monte Carlo integration. The main advantage of Latin Hypercube Sampling includes its characteristic of uniform stratification, which allows for obtaining tail sample values with fewer samples. This makes it particularly effective when dealing with large-scale data [9]. In general, Latin Hypercube Sampling is an effective stratified sampling technique that reduces the correlation between input variables by uniformly sampling in each dimension, thereby improving the accuracy and efficiency of model predictions. The whole optimization workflow is shown in Figure 12.

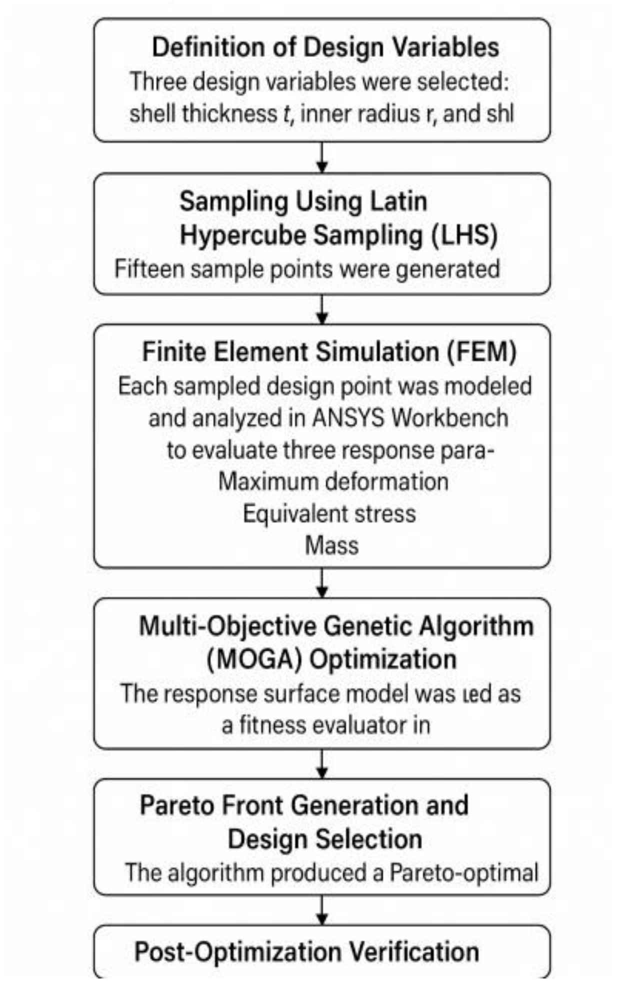

Figure12. Workflow of optimization

To clearly demonstrate the transition from sampling to optimization, Figure 12 presents the step-by-step workflow linking parameter sampling, simulation analysis, and multi-objective optimization using MOGA.

3.2 Variable settings

The volume and mass of the pressure hull occupy a significant proportion of the underwater robot, and to reduce the mass of the underwater robot and lower the cost, the design variables of the pressure hull can be sampled using the Latin Hypercube Sampling method, with the aim of selecting the optimal structural model. The optimization design variables selected this time are the shell thickness t, the inner diameter r, and the shell length d of the pressure hull. In the Design of Experiments, the three design variables t, r, and d are turned into input parameters, and the value ranges for these three variables are specified, as shown in Table 4.

Table 4. Variable settings

Variable	Initial Value	Minimum	Maximum
Thickness	4	3.6	4.4
Inner-radius	190	185	195
Length	400	390	410

When optimizing the shell, the accuracy assessment indicators of the model can be used for reflection, that is, the model's Coefficient of Determination, Root Mean Square Error, Relative Maximum Absolute Error, and Relative Average. Absolute Error. The relationship of the Coefficient of Determination can be expressed as:

$$\boldsymbol{R^2} = \mathbf{1} - \frac{\sum(y_i - \hat{y}_i)^2}{\sum(y_i - \bar{y})^2} \tag{8}$$

The formula n_i represents the number of experimental sample points, $\hat{\boldsymbol{y}}_{\boldsymbol{i}}$represents the model's predicted values, $\bar{\boldsymbol{y}}_{\boldsymbol{i}}$ represents the mean of the model's response values, y_i and represents the response value of the model's sample point. After completing the simulation calculations for all sample points, data fitting is performed on the sample points, as shown in Figures 13-15. The closer the value of the Coefficient of Determination is to 1, the higher the degree of fit between the predicted and actual values. Only when the predicted values have a high degree of fit with the actual values can subsequent multi-objective optimization be carried out. Table 5 summarizes the LHS test design.

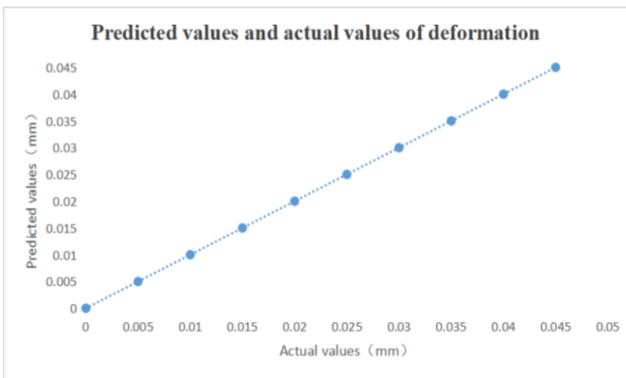

Figure 13. Predicted values and actual values of deformation

Table 5. LHS test design table

No	Thickness	Inner-radius	Length （mm）	Max-Def （mm）	Max-stress(MPa)	Mass （kg）
1	4.0000	190.0000	400.0000	0.0155	11.6573	2.9579
2	3.6000	190.0000	400.0000	0.0155	11.6573	2.9579
3	4.4000	190.0000	400.0000	0.0155	11.6573	2.9579
4	4.0000	185.0000	400.0000	0.0094	7.2708	4.6072
5	4.0000	195.0000	400.0000	0.0418	30.7766	1.2645
6	4.0000	190.0000	390.0000	0.0155	12.3072	2.8896
7	4.0000	190.0000	410.0000	0.0005	3.4185	3.0261
8	3.6748	185.9348	391.8697	0.0102	8.6356	4.2193
9	4.3252	185.9348	391.8697	0.0102	8.6356	4.2193
10	3.6748	194.0652	391.8697	0.0317	23.6728	1.5569
11	4.3252	194.0652	391.8697	0.0317	23.6728	1.5569
12	3.6748	185.9348	408.1303	0.0002	1.6694	4.3850
13	4.3252	185.9348	408.1303	0.0002	1.6694	4.3850
14	3.6748	194.0652	408.1303	0.0012	6.6635	1.6121
15	4.3252	194.0652	408.1303	0.0012	6.6635	1.6121

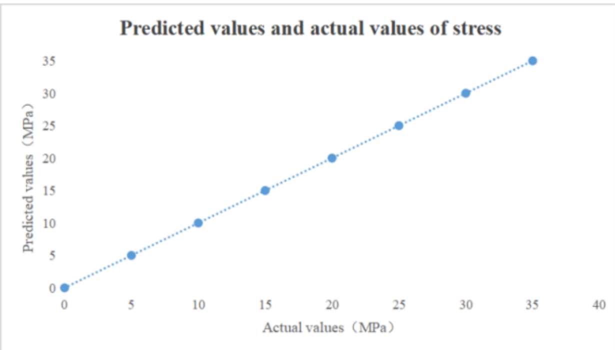

Figure 14. Predicted values and actual values of stress

From the above figures, it can be seen that the predicted values of the three items are close to the actual values. Therefore, the data of this model meets the requirements and can proceed with subsequent multi-objective optimization.

3.3 Multi-objective optimization of the pressure hull

In this optimization, the design variables are the shell thickness t, the inner diameter r, and the shell length d. The objective functions are the maximum deformation of the shell, the maximum equivalent stress, and the shell mass, aiming to minimize the mass to enhance speed and economic efficiency. When performing multi-objective optimization on the structure, each objective function is often contradictory. Therefore, in this paper, the allowable stress for the material 7075 aluminum alloy used for the shell is 328 MPa, and the working pressure is 0.5 MPa (at this time, the maximum deformation is 0.015 mm). Thus, the maximum deformation of the shell should be less than 0.015 mm, and the maximum equivalent stress should be less than 328 MPa, as shown in Figures 16, 17, and 18.

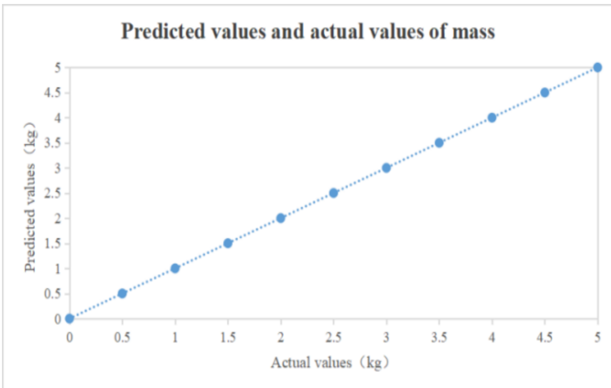

Figure 15. Predicted values and actual values of mass

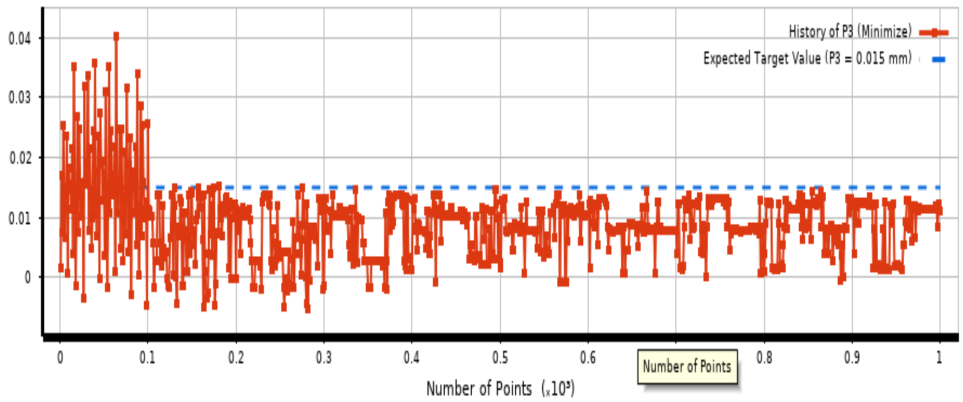

Figure 16. Maximum deformation iteration process

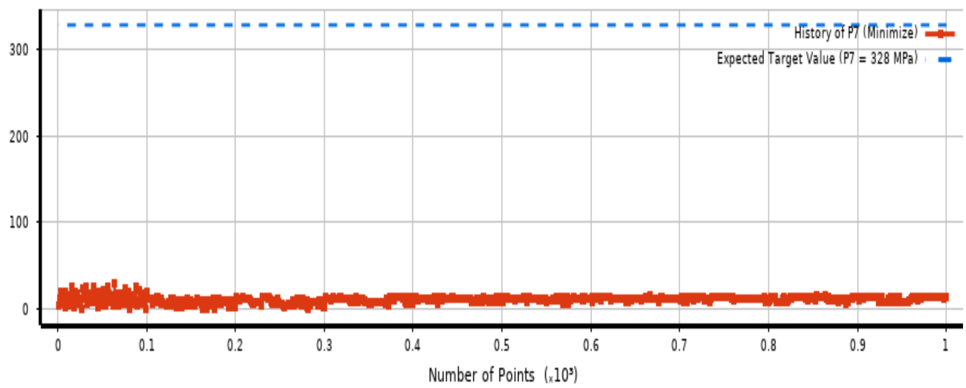

Figure 17. Maximum equivalent stress iteration process

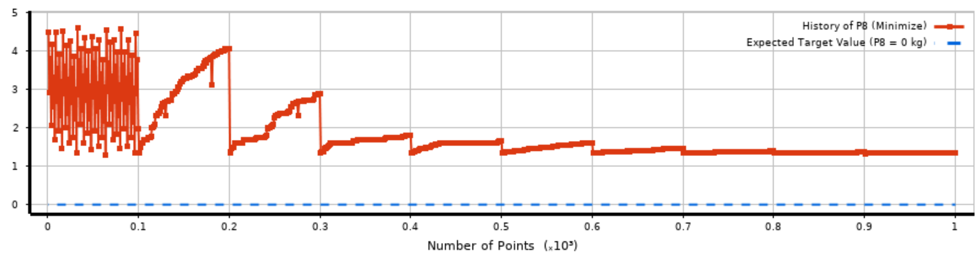

Figure 18. Mass iteration process

Table 6 summarizes the optimization objectives and constraints. The constraint on maximum deformation (<0.015 mm) is set based on the structural safety margin derived from initial simulations. The "superlative" weight assigned to mass reflects the design priority of minimizing overall hull weight to enhance maneuverability and endurance without compromising structural integrity. In the Optimization interface, 100 initial samples are selected, with each iteration having 100 samples, a maximum of 20 iterations, and 3 candidate points are retained. Utilizing the MOGA (Multi-Objective Genetic Algorithm) in the Workbench software, the optimized design candidate points, as shown in Table 7, are obtained. The iterative processes for maximum deformation, equivalent stress, and mass are illustrated in Figures 16 to 18.

Table 6. Weighted optimization settings

Objective Function	Optimization Objective	Weights
Max deformation	Minimum and less than 0.015 mm	Default value
Maxequivalent stress	Minimum and less than the allowable	Default value
Mass	Minimum	Superlative

It can be observed that the optimization process gradually converges over successive generations, reflecting the stability and effectiveness of the MOGA. Specifically, the deformation (Figure 16) and mass (Figure 18) consistently decrease, while the equivalent stress (Figure 17) fluctuates slightly but remains within the material's allowable stress limit of 328 MPa.

Table 7. Optimization design candidate points

Group	t（mm）	r（mm）	d（mm）	Deformation（mm）	Stress（MPa）	Mass（kg）
1	4.364	194.86	407.14	0.0090702	12.006	1.3312
2	4.3757	194.87	408.36	0.0041475	9.3082	1.3318
3	4.3681	194.86	406.48	0.0116442	13.421	1.3307

Table 8. Pre- and post-optimization adjustments of design variables

Design variables	Pre-Optimization(mm)	Post-Optimization(mm)	Adjust value（mm）
Thickness t	4	4.3681	4.4
Inner radius r	190	194.86	194.9
Length d	400	406.48	406.5

Table 9. Performance indicators of the pressure hull pre- and post-optimization

Performance indicators	Pre-Optimization（mm）	Post-Optimization（mm）	Comparison
Max deformation（mm）	0.01552	0.0116	-25.25%
Max equivalent stress（MPa）	11.657	13.421	15.13%
Mass（kg）	2.957	1.33	-54.78%

Figure 16 illustrates the convergence trend of maximum deformation across iterations, showing a steady decline until stabilization, which confirms the algorithm's effectiveness in minimizing structural displacement. Table 7 presents three optimized candidate solutions generated by the MOGA. All three solutions meet the required thresholds for stress and deformation. Among them, the second candidate (Group 2) achieves the lowest deformation and stress while maintaining minimal mass. The final design decision may favor this candidate due to its balanced trade-off between structural performance and lightweight efficiency. In the aforementioned three sets of data, neither the maximum deformation nor the maximum equivalent stress exceeds the required range. To achieve a lightweight pressure hull, it is more appropriate to select the schemes of the three sets of data. For the convenience of data optimization processing, as shown in the following Table 8. To verify the revised design variables, the design variable data is imported into Workbench for static analysis, and finally, the performance indicators before and after optimization are compared. The results are shown in Table 9. As shown in Table 9, the optimization process led to a significant mass reduction of 54.78%, from 2.957 kg to 1.33 kg. This improvement greatly benefits the AUV's energy efficiency and operating range. Meanwhile, the maximum deformation decreased by 25.25%, enhancing structural rigidity. Although the equivalent stress increased by 15.13%, it remains far below the material's yield strength, ensuring safe operation. These changes collectively demonstrate the success of the optimization strategy in achieving a robust, lightweight, and efficient pressure hull design.

From the above table, it can be concluded that the maximum deformation was reduced by 25.25%, the maximum equivalent stress increased by 15.13%, and the mass was reduced by 54.78%, which significantly decreased the mass of the pressure hull and improved agility.

4. Discussion

4.1 Innovation

Unlike prior studies that applied LHS or FEA independently, this work uniquely integrates LHS, FEM, and MOGA into a cohesive optimization framework tailored to shallow-water pressure hulls. This integration enables more efficient design space exploration and precise performance trade-offs. Compared to existing pressure hull optimization studies that utilize standard ANSYS-based simulations or Latin Hypercube Sampling (LHS) individually, this research integrates both LHS and a Multi-Objective Genetic Algorithm (MOGA) within a unified optimization framework. This combination allows for more comprehensive exploration of the design space, ensuring not only statistical robustness of the input variable distribution but also efficient convergence toward Pareto-optimal solutions. Unlike prior works that often focus on deep-sea or large-scale submersibles, this study specifically addresses shallow-water, small-scale AUVs, which face unique constraints in size, endurance, and deployment flexibility. The optimization process simultaneously targets three competing objectives—minimizing mass, controlling deformation, and limiting stress—while ensuring the structure meets modal safety and pressure resistance. Furthermore, this research contributes a clear design-to-validation workflow that bridges parametric modeling, statistical sampling, simulation-based optimization, and post-optimization evaluation. The inclusion of quantitative trade-off analysis (e.g., mass vs. stress vs. deformation) and the final selection of practical design candidates make this approach more application-oriented than many purely theoretical studies.

4.2 Validation and limitations of FEM simulation

While this study does not include direct experimental validation, several measures were taken to verify the credibility of the finite element analysis (FEA) results. First, the FEA boundary conditions, mesh quality, and pressure loading (0.5 MPa) were defined based on shallow-water operational profiles for AUVs and followed best practices in pressure vessel modeling. The pressure corresponds to approximately 50 meters of seawater depth, making the simulations realistic for near-surface missions. Second, the computed stress levels and deformation values were compared to analytical estimations using classical elasticity theory and Lamé equations. The results showed consistent trends, with safety factors above 2.5 under static loading. The results were benchmarked against literature values from recent works such as [13-15], where similar deformation, stress margins, and thicknesses were observed for aluminum and composite hulls under comparable loadings. Limitation: Physical testing—such as hydrostatic pressure chamber experiments—was not performed due to resource constraints. However, future work will include prototyping and experimental validation to strengthen design reliability.

5. Conclusion

This study investigated the lightweight optimization of a small submersible pressure hull for shallow-water AUVs using Finite Element Analysis (FEA), Latin Hypercube Sampling (LHS), and a Multi-Objective Genetic Algorithm (MOGA). The aim was to reduce structural mass while maintaining strength and safety under 0.5 MPa external pressure. Optimization results showed a 54.78% mass reduction, a 25.25% decrease in deformation, and a 15.13% controlled increase in stress, all within acceptable material limits. Modal analysis confirmed that the pressure hull avoided resonance risks, supporting structural integrity. The integrated design process enhanced the AUV's endurance and agility without sacrificing reliability. This methodology provides a practical reference for future small-scale underwater pressure vessel design in marine engineering.

Ethical issue

The authors are aware of and comply with best practices in publication ethics, specifically with regard to authorship (avoidance of guest authorship), dual submission, manipulation of figures, competing interests, and compliance with policies on research ethics. The author adheres to publication requirements that the submitted work is original and has not been published elsewhere.

Data availability statement

The manuscript contains all the data. However, more data will be available upon request from the authors.

Conflict of interest

The authors declare no potential conflict of interest.

References

[1] A. G. Q. Corpuz, J. P. Honra, A. D. Calderon, R. G. Tayactac and M. C. E. Manuel, "CFD Modeling and Optimization of Paint Hangar Overspray Filtration System," 2023 14th International Conference on Mechanical and Aerospace Engineering (ICMAE), Porto, Portugal, 2023, pp. 296-303, doi: 10.1109/ICMAE59650.2023.10424670.

[2] Li, S., & Calderon, A. D. (2024, June). Research Status and Development Trend of Precision Cutting Technology. In Journal of Physics: Conference Series (Vol. 2784, No. 1, p. 012025). IOP Publishing.doi:10.1088/1742 6596/2784/1/012025

[3] Liu, L., & Calderon, A. D. (2024, April). Optimization design of air filter housing structure based on computational fluid dynamics. In Third International Conference on Advanced Manufacturing Technology and Electronic Information (AMTEI 2023) (Vol. 13081, pp. 77-82). SPIE.https://doi.org/10.1117/12.3025790

[4] X. Liu, X. Wu, and A. D. Calderon, "Analysis and optimization of pre-stressed modal features of ship anchor support parts," Vibroengineering Procedia, Vol. 54, pp. 78–83, Apr. 2024,https://doi.org/10.21595/vp.2024.23831

[5] Macreadie, P. I., McLean, D. L., Thomson, P. G., Partridge, J. C., Jones, D. O., Gates, A. R., ... & Fowler, A. M. (2018). Eyes in the sea: unlocking the mysteries of the ocean using industrial, remotely operated vehicles (ROVs). Science of the Total Environment, 634, 1077 1091.https://doi.org/10.1016/j.scitotenv.2018.04.049

[6] S. Prabhakar and B. Buckham, "Dynamics modeling and control of a variable length remotely operated vehicle tether," Proceedings of OCEANS 2005 MTS/IEEE, Washington, DC, 2005, pp. 1255-1262 Vol. 2, doi: 10.1109/OCEANS.2005.1639927.

[7] G. E. Robles, E. C. R. Luna, R. G. Tayactac, J. P. Honra and A. D. Calderon, "Design and Aerodynamic Analysis of a Bio-inspired HAWT with Albatross and Stork Airfoil for Low Wind Velocity using CFD," 2022 6th International Conference on Power and Energy Engineering (ICPEE), Shanghai, China, 2022, pp. 37-46, doi: 10.1109/ICPEE56418.2022.10050316.

[8] Wei, L., Calderon, A. D., & Tian, P. (2024). Research on Ultrasonic Nondestructive Testing Algorithm for Metal Materials. In E3S Web of Conferences (Vol. 561, p. 03016). EDP Sciences.

[9] Zhang, L., & Calderon, A. D. (2024). Research and prospects of CNC lathe. Cogent Engineering, 11(1), 2299043.https://doi.org/10.1051/e3sconf/202456103016

[10] L. He, Y. Zhang, S.-z. Li, F.-r. Wang, Z.-h. Yuan, and Y. Bai,"Lightweight Design of Underwater Vehicle Pressure Shell Based on Kriging Model," in Proc. Int. Conf. on Autonomous Unmanned Systems (ICAUS 2022), pp. 2066–2077, Mar. 2023. DOI: 10.1007/978-981-99-0479-2_192

[11] X. Chen, L. Yu, L. Liu, L. Yang, S. Xu, and J. Wu, "Multi-objective shape optimization of autonomous underwater vehicle by coupling CFD simulation with genetic algorithm," Ocean Engineering, vol. (in press), Sep. 2023. DOI: 10.1016/j.oceaneng.2023.115722

[12] M. Imran, D. Shi, L. Tong, H. Waqas, R. Muhammad, and M. Uddin,"Design Optimization and Non Linear Buckling Analysis of Spherical Composite

Submersible Pressure Hull,"Materials, vol. 13, no. 11, 2439, May 2020.DOI: 10.3390/ma13112439
[13] Xu J, Kong X, Ge C, et al. Structural Design and Finite Element Simulation of Deep-Sea Pressure Resistant Electronic Cabin[C]//International Conference on Mechanical Manufacturing Technology and Material Engineering. Springer, Singapore, 2025: 376-382.
[14] Dama K K, Babu V S, Rao R N. State of the art on automotive lightweight body-in-white design[J]. Materials Today: Proceedings, 2018, 5(10): 20966-20971.https://doi.org/10.1016/j.matpr.2018.06.486
[15] He L, Zhang H, Zhang Y, et al. Lightweight Design of Underwater Vehicle Pressure Shell Based on Kriging Model[C]//International Conference on Autonomous Unmanned Systems. Singapore: Springer Nature Singapore, 2022: 2066-2077.
[16] Wang G, Zhao C, Pan P. Strength analysis of a semi-trailer tractor frame[R]. SAE Technical Paper, 2012. https://doi.org/10.4271/2012-01-0526

This article is an open-access article distributed under the terms and conditions of the Creative Commons Attribution (CC BY) license (https://creativecommons.org/licenses/by/4.0/).